Supporting Information

Ultrafast Carrier Thermalization and Cooling Dynamics in Few-Layer MoS_2

Zhaogang Nie,[a] Run Long,[b,c] Linfeng Sun,[d] Chung-Che Huang,[e] Jun Zhang,[f,g] Qihua Xiong,[f,g] Daniel W. Hewak,[e] Zexiang Shen,[d,f,h] Oleg V. Prezhdo,[b,] and Zhi-Heng Loh[a,f,*]*

[a] Division of Chemistry and Biological Chemistry, School of Physical and Mathematical Sciences, Nanyang Technological University, Singapore 637371, Singapore

[b] Department of Chemistry, University of Southern California, Los Angeles, California 90089, United States

[c] School of Physics, Complex Adaptive Systems Laboratory, University College Dublin, Belfield, Dublin 4, Ireland

[d] Centre for Disruptive Photonic Technologies, School of Physical and Mathematical Sciences, Nanyang Technological University, Singapore 637371, Singapore

[e] Optoelectronics Research Centre, University of Southampton, Southampton SO17 183, United Kingdom

[f] Division of Physics and Applied Physics, School of Physical and Mathematical Sciences, Nanyang Technological University, Singapore 637371, Singapore

[g] NOVITAS, Nanoelectronics Centre of Excellence, School of Electrical and Electronic Engineering, Nanyang Technological University, Singapore 639798

[h] Division of Materials Technology, School of Materials Science and Engineering, Nanyang Technological University, Singapore 639798, Singapore

[*] Address correspondence to: prezhdo@usc.edu (O.V.P.), zhiheng@ntu.edu.sg (Z.-H.L.)

1. Atomic-Force and Raman Microscopy Characterization of Five-Layer MoS_2 Sample

The homogeneity of CVD-grown sample is characterized by atomic-force microscopy (AFM, Veeco Dimension V) operated in the tapping mode. The AFM image collected over the central portion of the sample (Figure S1a) does not show any noticeable layer number changes, which should manifest itself as a height deviation of 0.65 nm. Scanning along the edge of the sample where the MoS_2 meets the substrate (Figure S1b) yields a step height of 3.46 nm (Figure S1c), in good agreement with that expected for a five-layer sample and an interlayer spacing of 0.65 nm. Further imaging of the sample by confocal Raman microscopy (WITec CRM200, 100× objective lens) reveals a high degree of homogeneity for both E^1_{2g} (Figure S1d) and A_{1g} modes (Figure S1e) . In these measurements, the excitation light is provided by a 532-nm laser. Raman images were generated by raster- scanning the sample with a step size of 250 nm. The spatial resolution is ~500 nm and the spectral resolution is ~1 cm^{-1}. Both AFM and Raman microscopy were performed over scan areas of 10×10 μm^2.

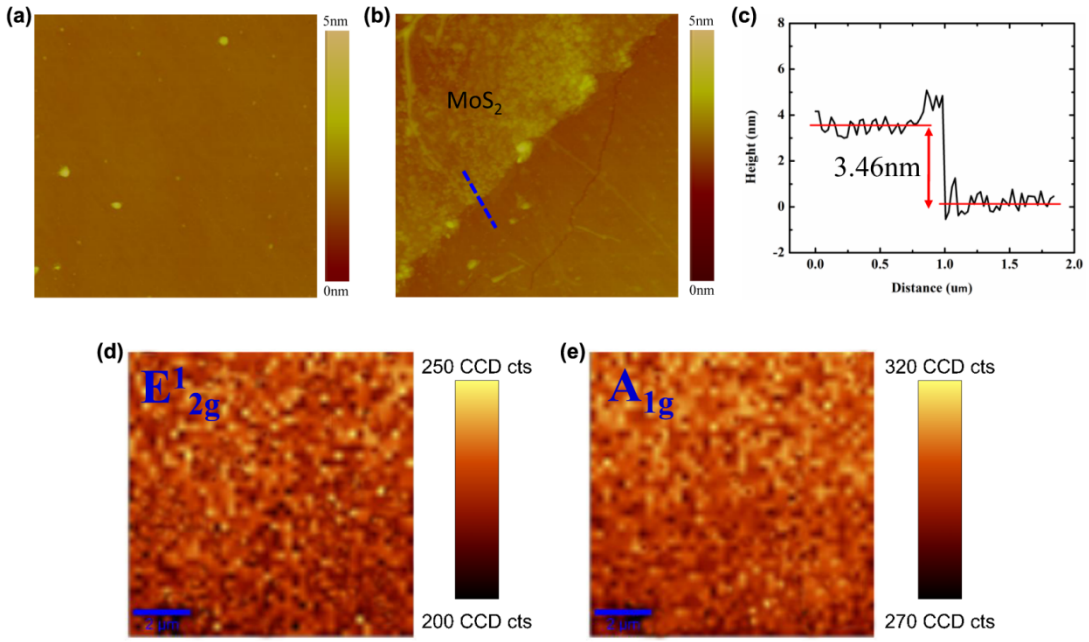

Figure S1. (a) AFM image collected in the central region of the sample, showing imperceptible height changes. (b) AFM image collected along the edge of the sample, where the MoS_2-coated region (labeled MoS_2) meets the substrate-only region. (c) The step height of 3.46 Å confirms the five-layer number of the sample. (d) Raman image of the E^1_{2g} phonon of MoS_2. (e) Raman image of the A_{1g} image of MoS_2. The area of all the AFM and Raman images is 10×10 μm^2.

2. Variable-Temperature Optical Absorption Spectroscopy of Five-Layer MoS_2

Variable-temperature optical absorption measurements in the temperature range of 77–340 K were performed with a UV/visible/NIR spectrophotometer (Perkin-Elmer Lambda950) equipped with a cryostat. The absorption spectra show distinct A and B excitonic transitions (Figure S2a). The absorption maxima of these transitions exhibit a red-shift with increasing temperature due to a combination of lattice expansion and electron-phonon coupling. The plot of absorption maxima

as a function of temperature *T* (Figure S2b) can be fit to the semi-empirical function of O'Donnell and Chen:

$$E_g(T) = E_g(0) - S\langle\hbar\omega\rangle\left(\coth\frac{\langle\hbar\omega\rangle}{2kT} - 1\right), \quad \text{(S1)}$$

where $E_g(T)$ is the energy gap of the electronic transition at *T*, $E_g(0)$ is the energy gap at absolute zero, *S* is the Huang-Rhys factor, and $\langle\hbar\omega\rangle$ is the average phonon energy.[1] The fit parameters are summarized in Table S1.

Table S1. Parameters extracted from the fits to the temperature-dependent absorption maxima of the A and B exciton transitions.

	Exciton A	**Exciton B**
$E_g(0)$ (eV)	1.865 ± 0.001	2.027 ± 0.001
S	1.736 ± 0.018	2.042 ± 0.024
$\langle\hbar\omega\rangle$ (meV)	24.6 ± 0.6	25.7 ± 0.7

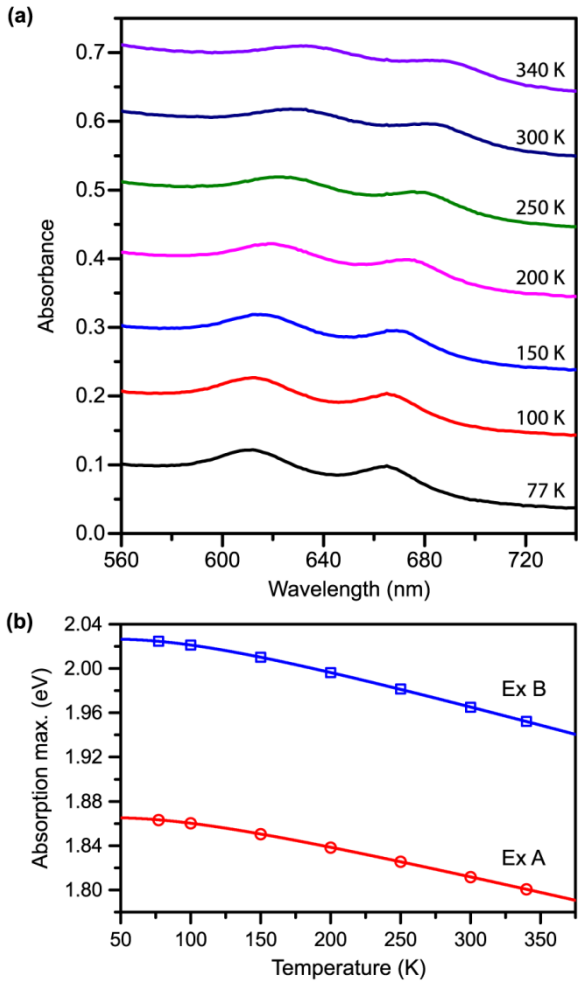

Figure S2. (a) Variable-temperature UV/visible absorption spectra of 5-layer MoS_2, showing two distinct peaks due to the A and B excitonic transitions. The spectra are offset by 0.1 absorbance unit for clarity. (b) Plot of the temperature-dependent absorption maxima of the A (○) and B (□) excitonic transitions. Solid lines are the fits to eq. S1.

3. Photoexcited Carrier Density and Absorbed Laser Spectrum Calculations

The carrier density can be calculated from the pump fluence and the optical absorption spectrum of the sample in the following way. The number of absorbed photons, and hence, the

number of electron-hole pairs that are produced by a given wavelength component λ of the broadband laser pulse is given by the absorbed laser spectrum $N(\lambda)$, where

$$N(\lambda) = N_{ph}(\lambda)\left[1 - 10^{-A(\lambda)}\right]. \quad \text{(S2)}$$

In the above expression, $N_{ph}(\lambda)$ is the number of photons at wavelength λ, calculated from the laser spectrum and the measured pulse energy, and $A(\lambda)$ is the absorbance of the sample at λ (see above). The normalized absorbed laser spectrum (Figure S3) resembles the experimental differential transmission spectra collected at short time delays (see Figure 3a of the main text), which suggests that the appearance of the experimental spectra at short time delays is due to the presence of a spectral hole. Integration of $N(\lambda)$ spectrally gives the total number of carriers produced by each pump pulse, which in turn yields the 2D carrier density for a given excitation focal spot size. For an excitation pump fluence of 0.33 mJ/cm^2 and a sample temperature of 77 K, our calculations result in an estimated 2D carrier density of 2.0×10^{13} cm^{-2}, or equivalently, an excitation fraction of 1.6%. For the range of pump fluences employed in our experiments, the 2D carrier densities are in the range of $(0.67–5.4)\times10^{13}$ cm^{-2} at 77 K.

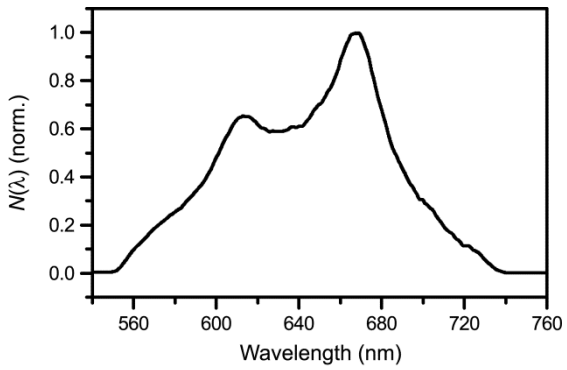

Figure S3. Normalized absorbed laser spectrum calculated for a temperature of 77 K.

Here, it is important to note that the spectral redshift of the MoS_2 optical absorption spectrum with increasing temperature also leads to a slight increase in the carrier density. This carrier density increase is due to the laser spectral density being higher at longer wavelengths (see Figure 1a of the main text). For a pump fluence of 0.33 mJ/cm^2, our calculations suggest that the carrier density increases from 2.0×10^{13} cm^{-2} to 2.4×10^{13} cm^{-2} as the temperature increases from 77 K to 340 K. This ~20% increase in carrier density, however, is insufficient to account for the rapid decrease in carrier thermalization time constant for sample temperatures ≥300 K (see Figure 3d of the main text).

4. Excitation Pump Fluence-Dependence Measurements and Photoexcited Carrier Density Calculations

Excitation pump fluence-dependence measurements were performed to verify that photoexcitation of the sample occurs in the one-photon regime. The experimental data shows that the peak differential transmission signal indeed scales linearly with the pump fluence (Figure S4).

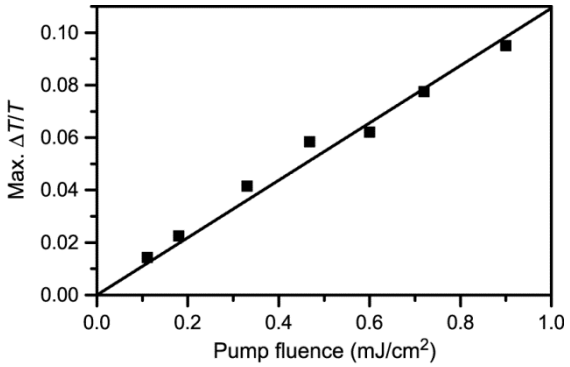

Figure S4. Dependence of the maximum $\Delta T/T$ signal on the excitation pump fluence. The linear fit confirms that photoexcitation occurs via a one-photon process.

5. Phonon Relaxation Timescale Measured by Long-Time Delay Scan

The focus of this work is the study of sub-picosecond dynamics of few-layer MoS_2. As such, the pump-probe time delay in most measurements is limited to 5 ps. Nevertheless, a time delay scan to 95 ps reveals slower dynamics, as shown in Figure S5 below. The time trace obtained at 667 nm, in the vicinity of the A excitonic transition, reveals a slow decay component with a time constant of 16.2 ± 0.2 ps, in addition to the 0.65 ± 0.01 ps component that is also observed in the 5-ps-long scans. We tentatively attribute the slow decay component to relaxation of optical phonons via anharmonic coupling to acoustic phonons.

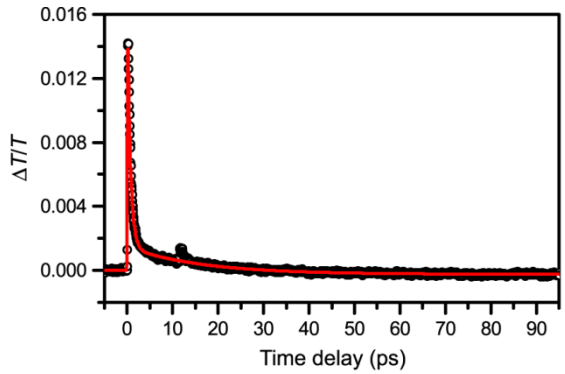

Figure S5. Time-resolved differential transmission probed at 667 nm, spanning a time delay range of –5 to 95 ps. The solid red line is the fit to a biexponential decay with time constants of 0.65 ± 0.01 ps and 16.2 ± 0.2 ps. Note that the bump at 12 ps is due to the etaloning effect that is caused by the 1.2-mm-thick fused silica substrate.

6. Measured Optical Pump-Probe Cross-Correlation

The time resolution of the experimental apparatus is measured by performing a second-order pump-probe intensity cross-correlation with a 10-μm-thick BBO crystal located at the sample

position. The resultant cross-correlation trace can be fit to a Gaussian function with a full-width at half-maximum (FWHM) of 14 fs (Figure S6), which corresponds to a laser pulse duration of 10 fs FWHM.

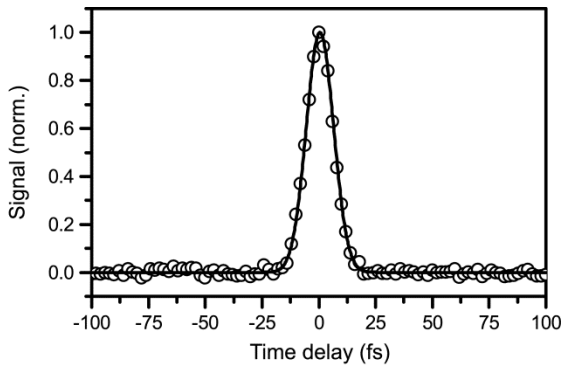

Figure S6. Cross-correlation trace of the pump and probe pulses. The solid line is a fit to a Gaussian function with a FWHM of 14 fs.

7. Suppression of Coherent Artifact by Singular Value Decomposition

In the vicinity of zero time delay, where the pump and probe pulses overlap, artifacts that are due to coherent phemomena such as transient grating, stimulated Raman, cross-phase modulation, and perturbed free-induction decay could arise. Along with scattering of the pump pulse into the probe pulse direction due to inhomogeneity of the sample surface, these artifacts could potentially obfuscate the analysis of time-resolved data at short pump-probe time delays. Ernsting and co-workers have shown that singular-value decomposition (SVD) of a two-dimensional probe wavelength-time delay dataset can effectively eliminate coherent artifacts.[2] Here, we show an example of an original dataset (Figure S7a) and the corresponding SVD-processed dataset (Figure S7b) to illustrate this point. In addition, the residual is also shown (Figure S7c). SVD essentially filters out coherent artifacts due to the dramatic difference

between the differential transmission spectrum of the MoS_2 sample and the spectral signature of the coherent artifact.

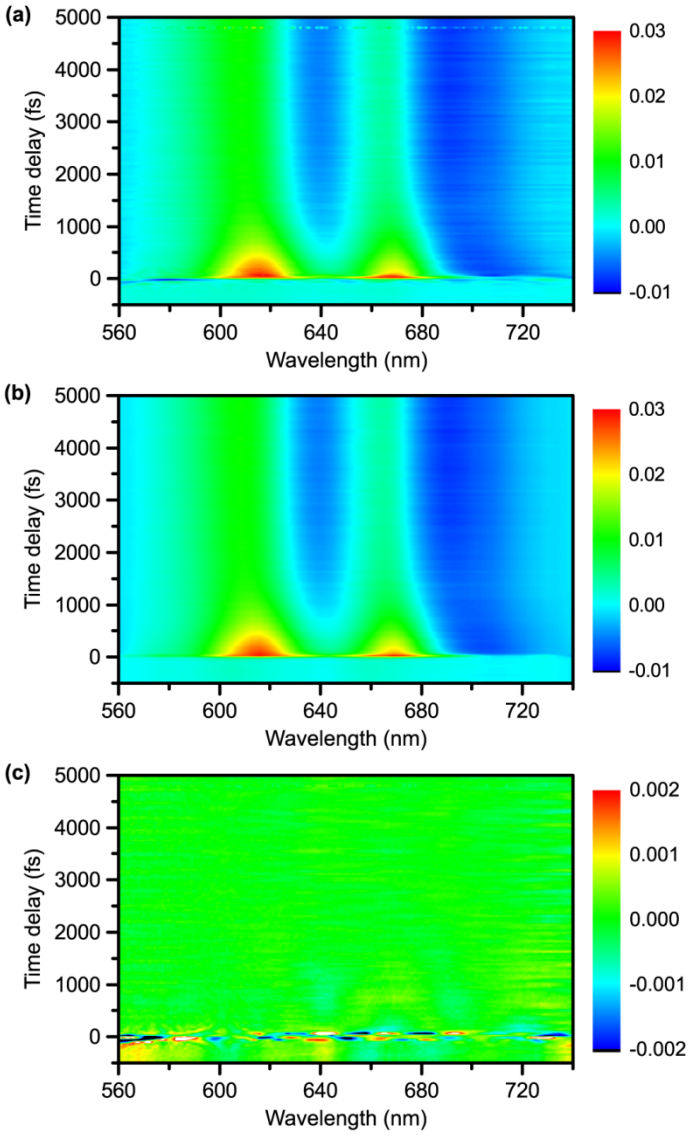

Figure S7. (a) Original dataset collected on five-layer MoS_2 at 77 K and with an excitation pump fluence of 0.33 mJ/cm^2. (b) The same data set as the above after the elimination of coherent artifacts by SVD. (c) The residual that shows the difference between the above two datasets, showing coherent artifacts near zero time delay. Note the different color scale.

8. Density of states calculations

The density of states of bilayer MoS_2 used in the time-domain density functional theory and nonadiabatic molecular dynamics simulations is shown in Figure S8.

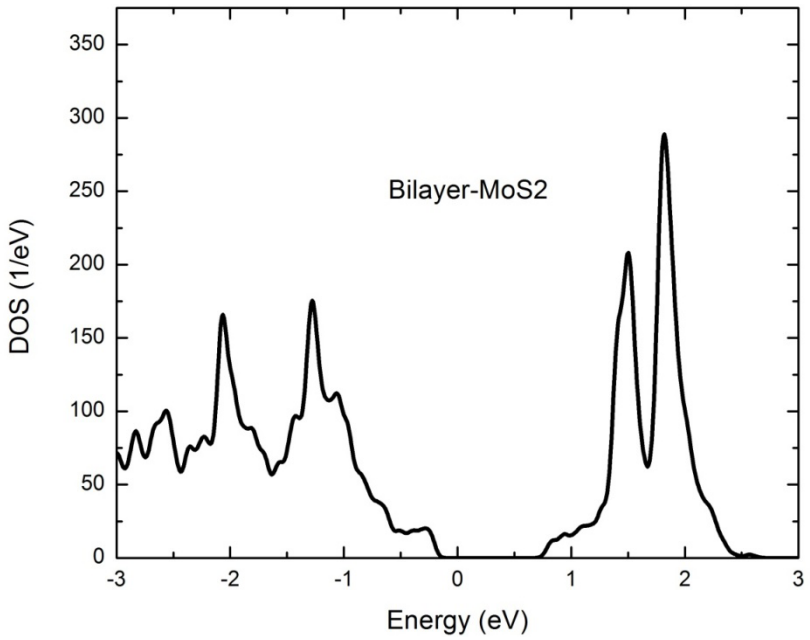

Figure S8. Density of states of the bilayer MoS_2 used in the *ab initio* nonadiabatic molecular dynamics calculation.

References

1. O'Donnell, K. P.; Chen, X. Temperature Dependence of Semiconductor Band Gaps. *Appl. Phys. Lett*. **1991**, *58*, 2924–2926.
2. Dobryakov, A. L.; Kovalenko, S. A.; Ernsting, N. P. Electronic and Vibrational Coherence Effects in Broadband Transient Absorption Spectroscopy with Chirped Supercontinuum Probing. *J. Chem. Phys*. **2003**, *119*, 988–1002.